Chaotic dynamics in erbium-doped fiber ring lasers

Henry D. I. Abarbanel,* Matthew B. Kennel,† Michael Buhl,‡ and Clifford Tureman Lewis‡

Institute for Nonlinear Science, University of California, San Diego, La Jolla, California 92093-0402

(Received 5 November 1998; revised manuscript received 25 January 1999)

Chaotically oscillating rare-earth-doped fiber ring lasers (DFRLs) may provide an attractive way to exploit the broad bandwidth available in an optical communications system. Recent theoretical and experimental investigations have successfully shown techniques to modulate information onto the wide-band chaotic oscillations, transmit that signal along an optical fiber, and demodulate the information at the receiver. We develop a theoretical model of a DFRL and discuss an efficient numerical simulation which includes intrinsic linear and nonlinear induced birefringence, both transverse polarizations, group velocity dispersion, and a finite gain bandwidth. We analyze first a configuration with a single loop of optical fiber containing the doped fiber amplifier, and then, as suggested by Roy and VanWiggeren, we investigate a system with two rings of optical fiber—one made of passive fiber alone.   The typical round-trip time for the passive optical ring connecting the erbium-doped amplifier to itself is 200 ns, so $\approx 10^5$ round-trips are required to see the slow effects of the population inversion dynamics in this laser system. Over this large number of round-trips, physical effects like GVD and the Kerr nonlinearity, which may appear small at our frequencies and laser powers via conventional estimates, may accumulate and dominate the dynamics. We demonstrate from our model that chaotic oscillations of the ring laser with parameters relevant to erbium-doped fibers arises from the nonlinear Kerr effect and not from interplay between the atomic population inversion and radiation dynamics. [S1050-2947(99)08607-2]

PACS number(s): 42.65.Sf, 42.55.Wd, 05.45.−a

I. INTRODUCTION

Rare-earth-doped fibers [1,2] appear very attractive for use as optical amplifiers in various stages of a communications system and as inline active elements in ring lasers used as transmitters and receivers in such a system. Erbium-doped lasers are especially attractive for long haul communications over optical fibers as the lasing wavelength, about 1550 nm, is near the minimum attenuation and dispersion point of standard single-mode optical fiber. The goal of using the baseband communications bandwidth of tens of terahertz (THz) around the carrier frequency of a few hundreds of THz might well be realized using a chaotic communications scheme in which the transmitter and receiver work over a very broad Fourier power spectrum while retaining sufficient state space structure to allow modulation and demodulation of information on the chaotic ''carrier'' (or courier) of information. The use of chaos as a ''courier'' of information is primarily for (1) effective utilization of the enormous bandwidth of these systems, and (2) the autosynchronization of the transmitter and receiver in the communications scheme we discuss.

This paper develops the theory of the operation in chaotic regimes of doped fiber ring lasers, especially those with parameters corresponding to doping with erbium. A communications window near 1300 nm is of some interest as well [3]. In addition to studying ring lasers with parameters associated with those of Er^{3+} doping as we do in this paper, in our future work we plan to analyze structurally similar ring lasers choosing parameters associated with Nd^{3+} and Pr^{3+} and doping where lasing at 1300 nm is seen [2].

We investigate models of doped fiber ring lasers (DFRLs). Such model equations have been discussed by Roy, Williams, and their collaborators [4,5], and they have shown, experimentally and theoretically, that chaotic field oscillations can be observed in these DFRLs. Roy and VanWiggeren [6] and our group [7] have shown experimentally and theoretically, respectively, that such ring laser systems can be used for communicating information from a transmitter laser to an open loop optical receiver. In work subsequent to that just cited, VanWiggerenm and Roy [8,9] extended their results to both higher symbol transmission rates and richer modulation schemes.

The main themes of this paper are the origin of chaos in the operation of erbium-doped fiber ring lasers and effective methods for solution of the relatively well known equations of motion for these lasers. These two issues are raised by the experiments of Roy and VanWiggeren [6] and possess substantial interest in themselves whether or not these laser systems turn out to be utilized in communications systems. The experiments of Roy and VanWiggeren demonstrate the presence of chaotic regimes in this kind of laser system, and a consideration of the time scales of the atomic lifetime (10 ms) and the ring round-trip time (≈ 100 ns) alone would suggest that in standard models of fiber lasers chaos would be absent.

The system, as we recall below, is basically that of a delay differential equation where the delay is the ring round-trip time and enters a map for the complex electric field amplitude and the differential equation describes the population inversion dynamics which is dictated by the fluores-

_____
*Also at Department of Physics, and Marine Physical Laboratory, Scripps Institution of Oceanography, UC San Diego. Electronic address: hdia@hamilton.ucsd.edu

†Electronic address: mkennel@ucsd.edu

‡Also at Department of Physics, UC San Diego. Electronic addresses: mbuhl@click.ucsd.edu (MB), ctl@click.ucsd.edu (CTL).

cence time scale of 10 ms which is much, much longer than this. An estimate based on this time scale alone would suggest that the population dynamics would be frozen out and the linear propagation of the field around the fiber ring would never yield chaos. This, if it were correct, would rule out these lasers as interesting for chaotic communications schemes as they would not be chaotic. Nonetheless, the experiments of Roy and VanWiggeren showed chaotic oscillations in their measurements of the output intensity of erbium-doped fiber ring lasers. The analysis we provide in this paper points clearly to the role of the nonlinear dependence of the polarization of the fused silica medium of the fiber as the source of the optical chaos. We test this quantitatively in the model we develop below, and we show that this chaos persists when we vary the difference of index of refraction between the electric field polarizations, the absorption for each polarization, and even the external injection of light into the cavity. None of these effects gives rise to chaotic oscillations in the absence of the medium nonlinearity, as expected, and each of them only slightly modifies the effect of the medium nonlinearity.

We present the results of a number of calculations relevant to the role of the nonlinear response of the medium. This nonlinear response is rather weak, and we show that it nevertheless is important as many hundreds of thousands of round-trips are required to build up the phenomena seen in the experiments. Even small quantities can accumulate significant effect in this case. With these results one can confidently proceed to investigate the coupling, possible synchronization, and transmission of information between two ring lasers of this variety. Again experiments have succeeded in showing many of the effects we seek to model, so the motivation for an accurate and efficient model is enhanced. The other dimension of this paper which adds substantially to earlier efforts is that of an efficient and accurate computational scheme applied to the relatively well known equations of motion. We describe this scheme in some detail as it should be of interest in further exploration of this class of laser systems as their use in communications is investigated.

In this paper and its companion [10] our focus is on investigating realistic models of the DFRL with an eye on the synchronization and communication aspects of the coupled chaotic optical devices. In our earlier work [7] we reported on results for what we called the ''Ikeda ring laser'' after the early investigations of Ikeda on ring lasers and the dynamics associated with the time delay in the travel time around the ring [11]. The Ikeda ring laser contained the essential ingredients of a ring laser communications system, and, in particular, we gave an analytic proof that two optical ring systems as described here will autosynchronize and allow accurate communication of information when the transmitter is run as a closed loop oscillator and the receiver is run as an open loop device. In that paper we ignored a variety of physical effects which play a significant role in the realistic operation of a rare-earth-doped fiber laser. These include direct pumping of the active medium by an external source; dynamics involving the two transverse polarizations arising from the vector nature of the electric field; properties of the optical fiber and other passive elements connecting the output back to the input of the rare-earth amplifier; intrinsic birefringence, the different indices of refraction, and hence

different velocities of signal propagation of orthogonal polarizations in realistic glass media; group velocity dispersion (GVD), a frequency-dependent change in the index of refraction; nonlinear birefringence, primarily, the cubic dependence of the atomic polarization on the electric field (Kerr effect); and the finite, and frequency-dependent gain bandwidth for a realistic active medium. The work in Ref. [4] developed models of erbium-doped lasers which included the first three of these items and serve as the predecessors to this work along with [7]. In this paper we address all of these issues as part of building a realistic model of a DFRL. The accompanying paper [10] addresses the coupling of these more realistic DFRLs, their synchronization properties, and their performance for communications. A fine review of fiber and semiconductor lasers and amplifiers has been published by van Tartwijk and Agrawal [12]. This review covers many of the topics touched on here and sets our investigation in the context of other investigations of these lasing media.

There are many suggestions in the literature on chaotic communications [13] that such systems provide secure communications. They may, and, equally, they may not. Security of communications is an entirely separate issue from the potential value to bandwidth utilization by such chaotic methods. In the discussion section of our subsequent paper [10] we will comment on the *cryptographic setting* of our communication methods [6,7,14] in hopes a rigorous analysis may be provided by others.

In this paper we formulate the equations of motion relevant to an erbium-doped fiber ring laser. In most conventional lasers, and in our earlier investigation [7], complex time-dependent dynamics arise from the interaction between cavity modes of the electric field and the population inversion in the active medium. A somewhat unusual feature of our present erbium-doped fiber laser system is that when the total fiber length, active and passive, in the optical ring is of the order of a few tens of meters, about 10^5 round-trips of light around the laser are required for the population inversion to play any role in the oscillations of the system. The fluorescence lifetime for the upper lasing state in Er^{+3}-doped silica is about 10 ms. We are primarily interested in fast gigahertz scale fluctuations, or equivalently in times well under sub-round-trip times because we wish to eventually convey information at this speed. At these shorter time scales, the population dynamics nearly ''freezes out'' and only serves to automatically set the overall gain and power levels. However, the dynamics are far from boring. Because of the unusually long cavity length and low losses, spatially complex electric field wave forms can propagate for long periods of time. This means that small physical effects which directly involve signals on the optical field, such as the dependence of the medium's polarization on electric field, group velocity dispersion [15], and the linear birefringence of silica glass can accumulate to large effects on the laser oscillations.

We begin by formulating the equations of motion. These consist of an ordinary differential equation for the population inversion and a set of partial differential equations for propagation of the two polarizations of the complex electric field through the active medium coupled with a four-dimensional map for these quantities describing their passage through the passive fiber. Altogether the solutions to the differential equations connect the complex fields at time t with the same

fields one round-trip time later at time $t + \tau_R$, and they describe the slow variation of the population inversion during any round-trip.

We then derive a propagation map, based on [4,5], reducing the solution of the partial differential equation to time delay maps, thus greatly diminishing the computational difficulty of the simulation. This differentiates our work from most of the conventional optical literature and is vital for our investigation because we need to be able to integrate hundreds of thousands of round-trips with high spatial resolution inside a single ring.

We present some characteristic numerical results for the dynamics of this system. In particular, by following nearby orbits in state space, we show that the Kerr nonlinearity gives rise to chaos in this system even when there is no driving by an external, detuned laser. When there is such driving, chaotic oscillations occur over a broad range of amplitudes and frequencies of the external source.

After the discussion of the single-ring DFRL we add another, passive ring, which introduces an additional time delay into the dynamics and results in chaotic oscillations with additional frequency components. This second ring was suggested by experiments of VanWiggeren and Roy [8].

Synchronization of two such ring lasers and communication of information modulated onto the chaotic signals carried between them is taken up in the accompanying paper [10].

II. DYNAMICAL EQUATIONS FOR THE DOPED FIBER RING LASER

We begin with a laser cavity composed of an active medium, rare-earth-doped fiber amplifier (DFA) of length l_A, whose output is connected back to the input by a single-mode fiber of length l_F. In the light path, we include an optical isolator to ensure unidirectional propagation, a polarization controller, and optionally, a fiber junction which connects an external monochromatic source which injects additional light into the ring. The center frequency of the optical signal in the cavity is ω_0, and the frequency of the injected light is ω_I. The coordinate around the ring is called z, and the length of the optical cavity is $L = l_A + l_F$. In this section we formulate the dynamical equations for this setup.

In a later section we add a ring of passive fiber to this. The reason for the second loop of fiber is that the ratio of fluorescence lifetime in the active medium to that of a round-trip time in the fiber ring is order 10^5 for an erbium amplifier so the population inversion dynamics is essentially time independent in such a system, leaving nearly linear dynamics for the electric field propagation. The only nonlinearity is that of the Kerr effect or cubic dependence of the material polarization on electric field. This weak nonlinearity *does* lead to chaotic oscillations of the erbium DFRL (EDFRL) as we will show here, but such oscillations occur on a time scale so long that they do not provide effective bandwidth utilization. The addition of a second ring of passive fiber, as suggested by VanWiggeren and Roy [8], gives us an additional time delay, allowing us to increase the frequency content of the chaotic signals. The single-ring configuration is illustrated in Fig. 1. In Fig. 2 we portray the situation with the second ring of passive fiber added.
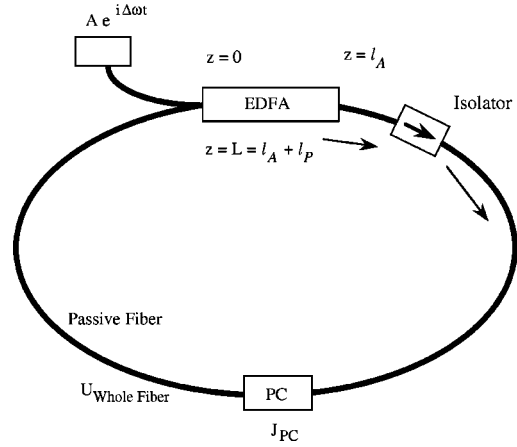

FIG. 1. Setup for our simulations of the dynamics of a rare-earth-doped fiber ring laser. An erbium-doped fiber amplifier with input at $z = 0$ extends to $z = l_A$. After leaving the amplifier light travels through an isolator which guarantees propagation only in the positive z direction, through a polarization controller, and through a length l_F of passive fiber described by $\mathbf{U}_{\text{whole fiber}}$. Just before the circulating light reenters the amplifier it receives external injection of light of amplitude $\mathcal{A}(t)$ and frequency $\Delta\omega$.

Following the derivations in [15] for the dynamics of the slowly varying envelope $\mathcal{E}(z,t) = (\mathcal{E}_x(z,t), \mathcal{E}_y(z,t))$ of the electric field, we find the wave equation for a birefringent wave guide in retarded coordinates $(z, \tau = t - z/v_g, k_0 = n_0\omega_0/c)$ to be

$$\frac{\partial \mathcal{E}_{x,y}(z,\tau)}{\partial z} + i\frac{\beta_2}{2}\frac{\partial^2 \mathcal{E}_{x,y}(z,\tau)}{\partial \tau^2}$$

$$= \pm \frac{ik_0\Delta}{2n_0^2}\mathcal{E}_{x,y}(z,\tau) \pm \frac{\Delta}{n_0 c}\frac{\partial \mathcal{E}_{x,y}(z,\tau)}{\partial \tau} + \frac{ik_0}{2n_0^2\epsilon_0}\mathcal{P}_{x,y}(z,\tau),$$
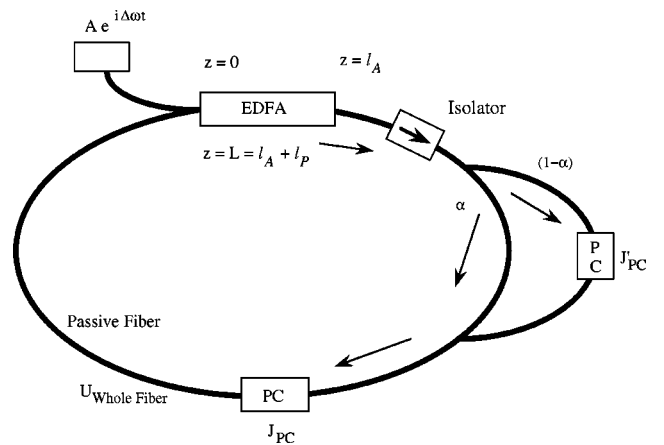
$$(1)$$

FIG. 2. Setup for our simulations of the dynamics of a rare-earth-doped fiber ring laser with two loops. As before, an erbium-doped fiber amplifier with input at $z = 0$ extends to $z = l_A$. In this setup, after the light leaves the isolator, some of the light is removed and passed though a second loop with a second polarization controller. After the light has been delayed a time τ_D by propagation around the second ring, it is reinjected back into the main loop.

where we use the upper choice in sign for x polarization and the lower for y. The group velocity dispersion coefficient $\beta_2 \approx -20$ ps^2/km at 1.55 μm in silica. The differential birefringence parameter is $\Delta = n_0(n_x - n_y)$. Compared to the familiar formulation in [15] we keep an additional time derivative in $\mathcal{E}$ on account of the birefringence because this influences the differential propagation speeds of *signals* in the different polarizations, not just the optical phase. Over many thousands of round-trips, this can be significant even if $\Delta \ll 1$. The material polarization $\mathcal{P}(z,t) = (\mathcal{P}_x(z,t), \mathcal{P}_y(z,t))$ has two important contributions: a polarization proportional to one power of the electric field $\mathcal{E}(z,t)$ arising from stimulated emission due to population inversion of the lasing atoms, and the Kerr nonlinearity proportional to three powers of $\mathcal{E}(z,t)$. This allows us to write

$$\mathcal{P}(z,t)/\epsilon_0 = \mathcal{P}_l(z,t) + \mathcal{P}_K(z,t), \qquad (2)$$

where

$$\mathcal{P}_{Kx}(z,t) = \chi_3 \left\{ \left(|\mathcal{E}_x(z,t)|^2 + \frac{2}{3}|\mathcal{E}_y(z,t)|^2 \right) \mathcal{E}_x(z,t) \right. $$
$$\left. + \frac{1}{3}\mathcal{E}_x^*(z,t)\mathcal{E}_y^2(z,t) \right\}$$

and

$$\mathcal{P}_{Ky}(z,t) = \chi_3 \left\{ \left(|\mathcal{E}_y(z,t)|^2 + \frac{2}{3}|\mathcal{E}_x(z,t)|^2 \right) \mathcal{E}_y(z,t) \right. $$
$$\left. + \frac{1}{3}\mathcal{E}_y^*(z,t)\mathcal{E}_x^2(z,t) \right\},$$

where we have identified the linear term in electric field $\mathcal{P}_l(z,t)$ and the nonlinear or Kerr term $\mathcal{P}_K(z,t)$ which we have written out explicitly.

To relate χ_3 to the more commonly measured macroscopic quantity, we temporarily concentrate on a single polarization of $\mathcal{E}$. Defining a power-dependent index of refraction $n = n_0 + n_2|\mathcal{E}|^2$, following the argument in [15] we find the following relation between n_2 and χ_3 $\chi_3 = 2n_2/A_{\text{eff}}$ where A_{eff} is the "effective" core area of the optical fiber, accounting for the transverse mode function. Using $n_2 \approx 1.2 \times 10^{-22}$ m^2/V^2 for ordinary fused silica glass and an effective area for the core of a single-mode fiber of $109\,(\mu\text{m})^2$ [9], we have a nominal value of $\chi_3 = 2.2 \times 10^{-12}$/V^2.

The linear term in the atomic polarization arises from the interaction between the electric field and the active lasing atoms. As discussed in [16] the erbium system is a three-"level" system in which a pump, for us an external diode laser running at 980 nm inside the amplifier, takes the $^4I_{15/2}$ ground state to the short lived $^4I_{11/2}$ excited state, from whence it rapidly goes to the long lived $^4I_{13/2}$ state where its fluorescence lifetime is 10.2 ms. The lasing transition is between this $^4I_{13/2}$ state and the $^4I_{15/2}$ state. Only the lasing transition between the $^4I_{13/2}$ and $^4I_{15/2}$ states is relevant to our discussion, so we treat the whole system as a pumped two-level system.

An erbium-doped fiber laser is class B, meaning that we can adiabatically eliminate the dynamics in the fast fluctuations in the polarization corresponding to the off-diagonal terms of the density matrix. These decay with a time scale $T_2 \approx 10^{-12}$ s. As we are not concerned with signal time scales that rapid, we assume the active atoms act as a resonantly driven dipole, providing a complex-valued electric susceptibility function depending on parameters such as the density of active atoms, their cross section, and the population inversion n [16]. In frequency domain the dipole response is an algebraic expression, $\mathcal{P}_l(\omega) = \chi_l(\omega,n)\mathcal{E}(\omega)$. For χ_l, we use for baseband signal frequencies $\omega \ll \omega_A$, following [17],

$$\chi_1(\omega,n) = \frac{\sigma \mathcal{N}c}{\omega_A} n(t) \left[\frac{\omega T_2 - i}{1 + \omega^2 T_2^2} \right], \qquad (3)$$

with σ an atomic cross section, and $\mathcal{N}$ the density of active atoms. The imaginary part of χ_1 contributes to gain, and the real part to a population-inversion-dependent change in the index of refraction. Absorbing the constants into a gain parameter g the resulting operator is $gn(\tau)/(1 + \omega^2 T_2^2)$, expressed in frequency space, which we separate and rearrange into the dominant zero-frequency gain $gn(\tau)$ and the frequency-dependent correction. We ignore the real part of χ_l in our simulation because it primarily corresponds to a secular change in the group velocity, equal for both polarizations, which we assume could be absorbed into v because in the equilibrium operation of an EDFRL, the fluctuations in $n(\tau)$ are very small compared to its average value.

We point out there is some confusion in the literature about the meaning of the "third-order nonlinearity" which arises from this term. Some experiments measure the phase shift induced by a long-term change (slower than T_1) in some applied electric field power. Running as a fiber amplifier, and not a ring, surely would change n very substantially, and via Re(χ_l) contribute to a large change in index of refraction which appears to change with input power, just as in the classical Kerr effect. However, for our study of communications in ring lasers, this is not important, as n changes far slower than the signal time scales we consider $O(10^{-9}$ s). We concern ourself only with χ_3 attached to a fast-responding Kerr nonlinearity.

The field's wave equations thus become

$$\frac{\partial \mathcal{E}_{x,y}(z,\tau)}{\partial z} = gn(\tau)\mathcal{E}_{x,y} + \mathbf{L}_{x,y}\mathcal{E}_{x,y} + \mathbf{N}_{x,y}\mathcal{E}_{x,y}. \qquad (4)$$

$\mathbf{L}$ contains the linear parts of the propagation operator excluding gain, and $\mathbf{N}$ the Kerr nonlinearity. The linear operator $\mathbf{L}$, including birefringence, GVD, and gain dispersion, is most naturally represented in the Fourier domain:

$$\mathbf{L}_{x,y} = \pm \frac{ik_0(n_x - n_y)}{2n_0} \mp \frac{\Delta}{n_0 c}i\omega - \frac{i}{2}\beta_2\omega^2$$
$$+ \frac{1 - gn(\tau)(1 + \omega^2 T_2^2)}{1 + \omega^2 T_2^2}, \qquad (5)$$

with ω the signal angular frequency, and assuming that $n(\tau)$ behaves as a very slowly varying (compared to signal frequencies ω) external parameter. The first term in $\mathbf{L}_{x,y}$ only

results in an overall arbitrary phase shift for the two polarizations, which can be absorbed without loss of generality into the polarization controller in the passive leg of the ring described in the next section. The term linear in ω represents linear birefringence; the next term, quadratic in ω, is the group velocity dispersion. The last term is associated with the gain curve, and arises from the fact that the center frequency of the line $\omega = 0$ is amplified more strongly than frequencies on either side of the line.

The nonlinear operators are

$$\mathbf{N}_x \mathcal{E}_x = \chi_3 \left\{ \left(|\mathcal{E}_x(z,\tau)|^2 + \frac{2}{3} |\mathcal{E}_y(z,\tau)|^2 \right) \mathcal{E}_x(z,\tau) \right.$$
$$\left. + \frac{1}{3} \mathcal{E}_x^*(z,\tau) \mathcal{E}_y(z,\tau)^2 \right\}, \tag{6}$$

$$\mathbf{N}_y \mathcal{E}_y = \chi_3 \left\{ \left(|\mathcal{E}_y(z,\tau)|^2 + \frac{2}{3} |\mathcal{E}_x(z,\tau)|^2 \right) \mathcal{E}_y(z,\tau) \right.$$
$$\left. + \frac{1}{3} \mathcal{E}_y^*(z,\tau) \mathcal{E}_x(z,\tau)^2 \right\}. \tag{7}$$

We have assumed the lasing gain g to be identical for both x and y polarizations. This appears to be true in the setup used by Roy and VanWiggeren [9]. The physical implication is that an erbium atom in the upper state has an equal cross section for lasing in both polarizations and that the pumping does not favor either state, and that the reservoir of inverted atoms is evenly shared.

These equations must be solved numerically to propagate the light from its entry into the DFA at $z = 0$ to its exit at $z = l_A$. From there we propagate the electric field around the remainder of the passive fiber. This process we take up now.

The electric field envelope at $z = l_A$ is related to the field at $z = 0$ by the symbolic expression

$$\mathcal{E}(z = l_A, t + l_A/v) = \mathsf{P}\{\mathcal{E}(z = 0, t)\}, \tag{8}$$

where we define P to be the propagation operator which transports the electric field from the beginning to the end of the active medium, an integration of the wave equations recently derived.

The polarization state of the field influenced by the random birefringence in the fiber arising from numerous small effects associated with imperfections in the fiber, strains, etc. Following [18] we write the net effect of passive fiber as a unitary Jones matrix which we denote $\mathbf{U}_{\text{whole fiber}}$,

$$\mathbf{U}_{\text{whole fiber}} = \begin{pmatrix} u_1 & u_2 \\ -u_2^* & u_1^* \end{pmatrix}, \tag{9}$$

where $|u_1|^2 + |u_2|^2 = 1$. An overall phase and an attenuation factor can be absorbed in the other terms to appear below. Similarly we associate a Jones matrix $\mathbf{J}_{\text{PC}}$ with the polarization controller.

Transporting this field from $z = l_A$ around the fiber and back to the input of the DFA at $z = L$ we have

$$\mathcal{E}(z = L, t + \tau_R) = (\mathbf{R} e^{i\omega_0 n_0 l_F/c} \mathbf{J}_{\text{PC}} \mathbf{U}_{\text{whole fiber}}) \mathsf{P}\{\mathcal{E}(z = 0, t)\}, \tag{10}$$

with $\tau_R = L/v_g$ the round-trip time for the full laser cavity, and $\mathbf{R}$ the matrix representing absorption by the fiber. In general the absorption in the two polarizations can be different, so we write

$$\mathbf{R} = \begin{pmatrix} R_x & 0 \\ 0 & R_y \end{pmatrix}, \tag{11}$$

$0 \leq R_x, R_y \leq 1$. The phase factor $e^{i\omega_0 n_0 l_F/c}$ comes from the free propagation from $z = l_A$ to $z = L$ over a distance l_F.

The points $z = 0$ and $z = L$ represent the same physical location, the input to the DFA. Dropping the label z on the field, henceforth implicitly referring only to $z = 0$, we have

$$\mathcal{E}(t + \tau_R) = (\mathbf{R} e^{i\omega_0 n_0 l_F/c} \mathbf{J}_{\text{PC}} \mathbf{U}_{\text{whole fiber}}) \mathsf{P}\{\mathcal{E}(t)\}. \tag{12}$$

Finally we add to this equation a term which represents injection of an externally generated electric field of complex amplitude

$$\mathcal{A}(t) = \begin{pmatrix} A_1(t) \\ A_2(t) \end{pmatrix}, \tag{13}$$

and frequency ω_I. This light is injected just before $z = 0$ where $\mathcal{E}(t)$ is defined, the entrance to the DFA. (See Fig. 1.) In the frame rotating at frequency ω_0, where we have written our equations, this changes the relation between $\mathcal{E}(t)$ and $\mathcal{E}(t + \tau_R)$ to

$$\mathcal{E}(t + \tau_R) = \mathcal{A}(t + \tau_R) e^{i(\omega_I - \omega_0)(t + \tau_R)}$$
$$+ (\mathbf{R} e^{i\omega_0 n_0 l_F/c} \mathbf{J}_{\text{PC}} \mathbf{U}_{\text{whole fiber}}) \mathsf{P}\{\mathcal{E}(t)\}. \tag{14}$$

This discrete-time map, a recursion relation between the field at time t and time τ_R later, is one of the dynamical rules of our ring laser system. The other is the population inversion equation in its simplified form.

The overall phase factor and Jones matrix of the real fiber are unknown and without loss of generality we can absorb them into $\mathbf{J}_{\text{PC}}$. Any such matrix may be parametrized by three angles $\theta_1, \theta_2, \theta_3$. In experimental circumstances, the absolute values of these angles are unknown, although they may be varied by rotating the appropriate optical elements of the polarization controller.

III. SOLUTION OF THE ELECTRIC-FIELD PROPAGATION EQUATIONS

We integrate the equations of motion using a time step δt which is a small fraction of the round-trip time τ_R: $\delta t = \tau_R/N_s$, $N_s = 2500$. The dynamics of the population inversion is given by an ordinary differential equation which can be integrated by conventional means at each integration time step δt. Because the propagation map (14) connects electric fields a full τ_R later, we must save a rolling buffer N_s steps long for the complex coefficients of the electric field $\mathcal{E}_x$ and $\mathcal{E}_y$.

At each time step, we recall the values of $\mathcal{E}_x(t)$ and $\mathcal{E}_y(t)$ and operate on them with maps representing propagation through the active medium followed by the passive components of the ring, then we store the future values as $\mathcal{E}_x(t + \tau_R)$ and $\mathcal{E}_y(t + \tau_R)$ in the buffer. Now time advances for-

ward by δt. We recall $\mathcal{E}_x(t+\delta t)$ and $\mathcal{E}_y(t+\delta t)$, and we repeat. The map propagating the field through the passive fiber is given explicitly by Eq. (14). We now discuss the transformation of the partial differential equations (4) into maps propagating the electric field from the beginning of the active medium to the end of the active medium in one operation, just as we used the Jones matrices for the passive section of fiber.

In the time-asymptotic operation with realistic parameters corresponding to erbium-doped fiber lasers, neither **L** nor **N** has a substantial influence in any *single* pass through the lengths of active medium typically found in a commercial EDFA: $l_A \approx 20$ m. The dominant effect in the active medium is gain, balanced by the net attenuation found in the rest of the ring. This means that we can approximate the solution of the differential equation (4) which simultaneously includes all three operators **L**, **N**, and $gn(t)$ by operating on $\mathcal{E}$ by each of the operators in turn. Each can be easily solved to find $\mathcal{E}$ at $z=l_A$, given $\mathcal{E}$ at $z=0$.

In an erbium-doped amplifier, the gain curve is very broad. That is, $T_2\omega \ll 1$ for the signal frequencies we may resolve with our spatial discretization of the loop. More precisely, we can resolve a maximum frequency about 5 GHz in the present computation while $1/T_2 \approx 1000$ GHz.

The differential equation $\partial \mathcal{E}/\partial z = \mathbf{L}\mathcal{E}$ is solved by $\mathcal{E}(z=l_A)=\exp(l_A \mathbf{L})\,\mathcal{E}(z=0)$, and this has a simple representation in the frequency domain. Operationally, we take a chunk of $\mathcal{E}$ from the buffer 2^M steps long ($2^M \ll N$), transform to frequency domain by a fast fourier transform (FFT), apply the operator $\exp(l_A \mathbf{L})$, transform to real space, and save these values, denoted $\mathcal{E}_{x,y;L}$ in new buffers. A certain number of points from each end are discarded before the result is saved in the $\mathcal{E}_{x,y;L}$ auxiliary buffer in order to account for end effects which can bedevil Fourier-based methods. The frequency-dependent term in the solution is expanded in powers of ω into $1 - g l_A n(t) T_2^2 \omega^2$ to simplify computations. This form more clearly demonstrates the decreased gain for frequencies further from the center of the line at $\omega=0$. The remaining imaginary terms of **L** apply a frequency-dependent phase shift, i.e., dispersion, but not dissipation. Explicitly,

$$\mathcal{E}_{x,y;L}(\omega,z=l_A) = [1 - g l_A n(\tau) T_2^2 \omega^2]$$
$$\times \exp\left(\mp i \frac{\Delta l_A}{n_0 c}\omega - i \frac{\beta_2 l_A}{2}\omega^2 \right)$$
$$\times \mathcal{E}_{x,y}(\omega,z=0). \quad (15)$$

The value of $n(\tau)$ is assumed to be constant during the application of this linear operator, fixed to the current value at the beginning of the domain. In the asymptotic equilibrium state for an erbium-doped fiber laser, the population inversion changes negligibly during a single traversal of the active medium.

This process of reading in points from the $\mathcal{E}$ buffer, operating on them with the linear operator, and saving them in the auxiliary buffer happens independently from the main integration loop: a counter keeps track of the latest point in time which has been saved in $\mathcal{E}_{x,y;L}$, and, if it is less than the "current time" in the main loop, an additional chunk is pro-

cessed. The number of sites in the loop N_s is not the same as for the FFT computation, unlike many existing optical simulations in the literature. Integration strictly with the FFT assumes periodic boundary conditions. Much of the existing literature is only concerned with repetitive pulses, and only for a single polarization (or examining only intensity), in which case the identification of the entire loop with the FFT input is acceptable, allowing one to advance an entire round-trip per large integration step. In our situation, however, that approach is inappropriate because we consider both polarizations, and the polarization controller strongly rotates the axes and the attenuation is different between the axes.

Other than the evaluation of the linear operator, the remainder of the integration algorithm proceeds strictly pointwise, taking the envelope values stored in $\mathcal{E}_{x,y;L}(t)$, operating on them with the nonlinear Kerr operator, the gain operator, the passive components of the ring (polarization controller, attenuation, external driving), and storing it in the buffer as $\mathcal{E}_{x,y}(t+\tau_R)$. $n(t)$ is updated with a simple Euler integration formula, and time advanced one discrete step to $t+\delta t$.

The Kerr integration is also approximate. For realistic lengths of active medium and birefringences, there are significant phase oscillations between the x and y components, which result in the last terms in Eq. (6) averaging to zero. This approximation is valid when propagating through characteristic lengths much larger than the modal "beat length" $L_B = \lambda/|n_x - n_y|$ [15]. We estimate $L_B \approx 1$ m whereas our active medium l_A is about 20 m. In this standard approximation, the result is an intensity-dependent nonlinear phase change:

$$\mathcal{E}_x(z=l_A) = \exp\left[i\, l_A \chi_3 \left(|\mathcal{E}_x|^2 + \frac{2}{3}|\mathcal{E}_y|^2 \right) \right] \mathcal{E}_x(z=0),$$
$$(16)$$
$$\mathcal{E}_y(z=l_A) = \exp\left[i\, l_A \chi_3 \left(|\mathcal{E}_y|^2 + \frac{2}{3}|\mathcal{E}_x|^2 \right) \right] \mathcal{E}_y(z=0).$$

The full solution has been computed in the literature [19] and involves Jacobi elliptic functions. The gain part of the propagation equation,

$$\frac{\partial \mathcal{E}(z,\tau)}{\partial z} = g n(z,\tau)\mathcal{E}(z,\tau), \quad (17)$$

has the solution

$$\mathcal{E}(z,\tau) = \exp\left[g \int_0^z dz'\, n(\tau,z') \right] \mathcal{E}(z=0,\tau). \quad (18)$$

Given the electric field at the start of the active medium $\mathcal{E}(z=0,\tau)$ we have a formula giving its value at the end of the active medium whose only other time dependence is the population inversion averaged over the medium:

$$\mathcal{E}(l_A,\tau) = e^{g l_A w(\tau)}\mathcal{E}(z=0,\tau), \quad (19)$$

where

$$w(\tau) = 1/l_A \int_0^{l_A} dz'\, n(z',\tau). \quad (20)$$

The physics of the atomic polarization in the active medium is governed by external pumping, spontaneous emission, and stimulated emission from the light propagating through it. This is described by the usual Bloch equations for the population inversion at time τ and spatial location z:

$$\frac{\partial n(z,\tau)}{\partial \tau} = \text{pumping term} - \frac{1}{T_1}[n(z,\tau)+1]$$
$$- \xi n(z,\tau)|\mathcal{E}(z,\tau)|^2, \qquad (21)$$

with T_1 the lifetime of the excited state (10 ms for a typical EDFRL) and ξ a constant relating to the optical cross section governing the transition rate between levels. With the solution (18) and assuming real g we can integrate Eq. (21) by $l_A^{-1}\int_0^{l_A}dz'$ to arrive at the dynamics for the population inversion averaged over the entire active medium $w(\tau)$ $= w(l_A,\tau)$, following Ref. [4],

$$\frac{dw(\tau)}{d\tau} = Q - \gamma[w(\tau)+1+(e^{2l_A g w(\tau)}-1)|\mathcal{E}(z=0,\tau)|^2], \qquad (22)$$

here with time units rescaled by the round-trip time τ_R.

This scalar quantity $w(\tau)$ is the only representation of the population inversion state needed in the simulation. It is important to note that the magnitude $|\mathcal{E}|^2$ is preserved by our propagation operations, except for the gain term, including the nonlinear Kerr phase shifts. After the Kerr operator, the main component of the gain is applied to the two complex envelopes, multiplying each by $\exp[g l_A w(\tau)]$, and finally we account for the passive components of the ring, to produce $\mathcal{E}_{x,y}(t+\tau_R)$.

IV. EXAMPLES OF THE EDFRL OPERATION

Using the numerical methods just described we have evaluated the dynamics of the model DFRLs derived earlier. In these calculations we employed 2500 locations around the ring as points to sample the electric field. This corresponds to $\tau_R/2500$ or a time resolution of about 0.08 ns. We should resolve fluctuations in electric field or light intensity up to 5 or 6 GHz with this integration scheme. The experiments are presently able to resolve about 1 GHz fluctuations with the diode detectors available.

The only power-dependent dynamical quantity is the size of the third-order nonlinearity, which is is most easily characterized by the nondimensional nonlinear phase shift Φ_{nl} experienced by an $\mathcal{E}$ field as it passes through the fiber is given by [15]

$$\Phi_{nl} = \frac{2\pi n_2 L}{\lambda A_{eff}}(P_a + 2P_b), \qquad (23)$$

where P_a, P_b are the optical powers in the parallel and perpendicular direction.

In a typical experimental case [9] running at a pump level of 20 times threshold, a typical output power is 136 mW. Splitting the power equally between polarizations and estimating a total fiber length L of 40 m, we estimate an induced nonlinear phase shift as

$$\Phi_{nl} = \frac{2\pi(3.2\times10^{-20}\ \text{m}^2/\text{W})(40\ \text{m})}{(1.55\ \mu\text{m})(109\times10^{-12}\ \text{m}^2)}\left(\frac{3}{2}(136\times10^{-3}\ \text{W})\right) \qquad (24)$$

$$\simeq 10^{-2}. \qquad (25)$$

This is the phase shift associated with one round-trip through the fiber cavity. In our work we investigate the results of hundreds of thousands of round-trips around the cavity, and thus the effects of a Φ_{nl} of this size can be quite substantial.

We parametrize our dynamical simulations by Φ_{nl}, the only dynamically relevant combination of power and nonlinearity. Physically this could be interpreted as varying the EDFA pump level, linearly increasing the optical power above threshold, or varying the length of the fiber cavity L. The remaining parameters in the definition of Φ_{nl} are assumed to be generally fixed in any given experiment. Each calculation allowed the ring laser to run for 500 000 round-trips before the dynamics was observed. This is relevant to erbium-doped fiber lasers where the lifetime of the upper lasing state is about 10 ms and approximately 100 000 round-trips are required for the population inversion dynamics to play a role. The pumping level for the population inversion equation was a few times above threshold, and the dissipation in x polarization and y polarization was taken to differ by about 5% and each to be about 0.9 on each round-trip. The size of Φ_{nl} was chosen to be 1.5×10^{-2}, a slight increase on the above nominal value. The difference in indices of refraction was taken to be about 10^{-6} (see Table I).

In Fig. 3 we show a typical time series for the total intensity with a single loop of passive fiber. The top graph shows the intensity at frequencies up to 6 GHz. In the experiments of Roy and co-workers [20] a photodiode used to measure the intensity cannot resolve frequencies above 1 GHz. So that our results will have the same frequency content as the experiment we passed the same data through a single pole filter to simulate the photodiode, a high-order far infrared (FIR) filter to simulate the analog to digital converter in the oscilloscope, and down sampled to 1 GHz. This time series is shown in the middle of Fig. 3. Underneath is an experimental time series from the laser of Roy and co-workers [20].

The amplifier was pumped at 20 times the lasing threshold of the ring and there is no external injection, although typically the addition of external injection does not qualita-

TABLE I. Typical parameters for our EDFRL model simulations.

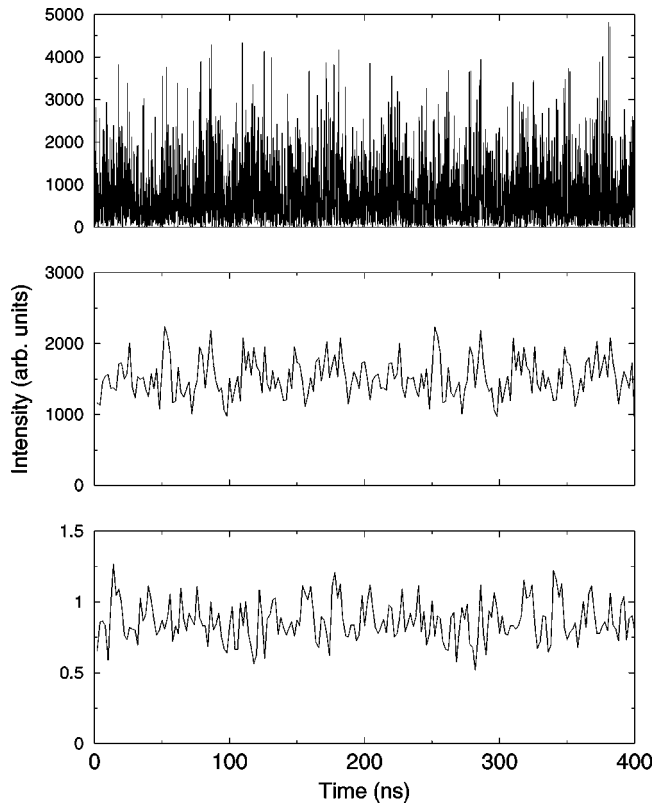| Quantity	Symbol	Value
Linear modal birefringence	$n_x - n_y$	1.8×10^{-6}
Pump strength	Q	3.4×10^{-3}
Gain times active length	$g l_A$	0.675×10^{-2}
Ratio of round-trip time to erbium lifetime	γ	10^{-5}
Round-trip time	τ_R	200 ns
Polarization dephasing time	T_2	1 ps
GVD coefficient	β_2	$-20\ \text{ps}^2/\text{km}$
Length of active medium	l_A	20 m
Nonlinear phase shift	Φ_{nl}	1.5×10^{-2}

FIG. 3. Top: A time series of the output of the laser simulation sampled at 12.5 GHz. This is a laser with a single loop and no external injection. Here, $\Delta n \approx 2.0 \times 10^{-6}$, $\Phi_{nl} = 1.5 \times 10^{-2}$, and the reflectances are $R_x = 0.9$, and $R_y = 0.85$. Middle: The same data after a filter to simulate a photodiode and down sampled to 1 GHz. Bottom: An experimental time series from Roy and VanWiggeren also sampled at 1 GHz.

tively change the dynamics. The round-trip time in the simulations was 200 ns, while in the experiment it is 186 ns. Figure 4 displays the Fourier power spectrum on two scales for the total intensity displayed in Fig. 3. Notice that because the time scale of light to go around the cavity is much smaller than the time scale for the population inversion or any dynamics from Φ_{nl} most of the power is concentrated into harmonics of one round-trip. In order to see any dynamics on these time scales we can change the sampling period to be equal to τ_R, removing any changes within one round-trip. A time series down sampled thus is given in Fig. 5. Here we can see that, although the intensity appears to be mostly periodic from round-trip to round-trip, on long time scales there are aperiodic fluctuations.

In the future we plan to analyze these time series along with the experimental time series of Roy and co-workers [20] using well tested nonlinear analysis tools [21].

V. CHAOS IN THE ONE-RING EDFRL

The EDFRL model described above represents an extremely high-dimensional system. In our simulation, the equations are integrated by separating the ring into 2500 discrete-time steps. Each time step contains four electric field variables, $\mathrm{Re}\,\mathcal{E}_x$, $\mathrm{Im}\,\mathcal{E}_x$, $\mathrm{Re}\,\mathcal{E}_y$, and $\mathrm{Im}\,\mathcal{E}_y$. These, along with the constantly changing population inversion variable $w(t) = n(t) l_A$, results in 10 001 state variables in the system.
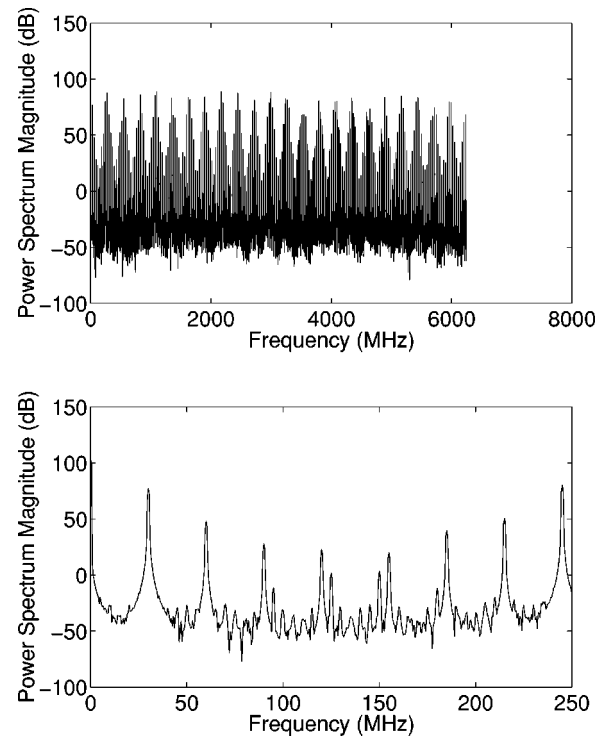
FIG. 4. Power spectrum of the output of the laser simulation. The original time series was sampled at 2500 per τ_R. This is a laser with a single loop and no external injection. Here, $\Delta n \approx 2.0 \times 10^{-6}$, $\Phi_{nl} = 1.5 \times 10^{-2}$, and the reflectances are $R_x = 0.9$ and $R_y = 0.85$.

At each time step, the electric field variables are coupled not only to the previous round-trip variables, but also with their neighbors through the population inversion dynamics, GVD, and linear birefringence effects. The complexity of the integration algorithm, especially the spectral evaluation of the linear propagator, makes a direct computation of the full spectrum of Lyapunov exponents (as was done in [7]) impractical as one would need to take Jacobians of the one-time-step map implied by the integration algorithm. How-
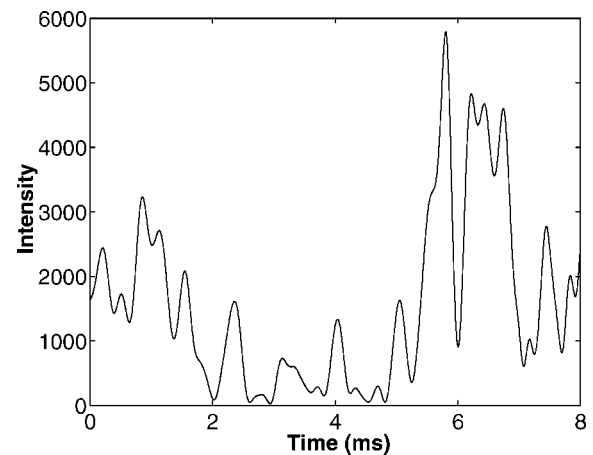

FIG. 5. Time series of the output of the laser simulation. This was only sampled once per τ_R to remove the fast sub-round-trip fluctuations. As before, this is a laser with a single loop and no external injection. Here, $\Delta n \approx 2.0 \times 10^{-6}$, $\Phi_{nl} = 1.5 \times 10^{-2}$, and the reflectances are $R_x = 0.9$ and $R_y = 0.85$.

ever, one may estimate the largest Lyapunov exponent through the rate of divergence of nearby trajectories.

One EDFRL, called laser A, is integrated for 5×10^5 round-trips (equal to about 1/10 of a second in real time) to reach what appears to be asymptotic behavior. At this point, a second (identical) laser, called laser B, with identical physical parameters is initialized with identical state variables as laser A, with B's electric fields $\mathcal{E}_B$ perturbed by a very small amount of noise, knocking it slightly off of the trajectory of laser A. The noise is added to both the real and imaginary parts of $\mathcal{E}_B$ in both components, Gaussian distributed with a variance of size ϵ which is set as an external parameter of the simulation. In the following simulations, ϵ is a factor of 10^{-4} smaller than the average magnitude of the electric field components.

Concrete computation of Lyapunov exponents from trajectory divergences requires a metric to be chosen. The metric we use here is

$$\mathcal{D}_1 = L^{-1} \int_0^L dz |\mathcal{E}_{x_A}(z) - \mathcal{E}_{x_B}(z)|^2 + |\mathcal{E}_{y_A}(z) - \mathcal{E}_{y_B}(z)|^2,$$
(26)

with L corresponding to a full round-trip. This metric measures the difference in each electric field component and then calculates the squared distance in a four-dimensional Euclidean manner. This metric is sensitive to phase deviation intensity and polarization differences.

For an optical system, what is measured experimentally is in many cases a projection of the general state space of the system into a certain physically meaningful subspace. An example is the detection of optical intensity by a photodiode. This measurement would read the intensity of the electric field wave, but by itself says nothing of the optical phase or details about the polarization of the wave. Consequently, if one uses a polarization insensitive photodiode to record a chaotic time series of electric field intensity, one cannot say anything regarding the phase chaos in their data set without further tools. In order to connect our simulation to this physical circumstance, we also examine a metric which is sensitive only to intensity differences. It is conceivable that nonlinearity produced by the Kerr effect, for instance, might only cause chaotic polarization or phase differences and not lead to chaotic amplitude fluctuations.

The first metric, $\mathcal{D}_1$, is sensitive to both phase and intensity divergences, but the second metric,

$$\mathcal{D}_2 = L^{-1} \int_0^L dz |[|\mathcal{E}_{x_A}(z)|^2 + |\mathcal{E}_{y_A}(z)|^2]$$
$$- [|\mathcal{E}_{x_B}(z)|^2 + |\mathcal{E}_{y_B}(z)|^2]|,$$
(27)

only responds to intensity differences. Because the projections of the full $\mathcal{E}(z)$ space down to the $|\mathcal{E}(z)|$ intensity space is not invertible, the Lyapunov exponents need not be the same. Intensity is more experimentally accessible, making this particular projection interesting.

We quantify the divergence of nearby orbits in the largest Lyapunov exponent of the system which is defined by

$$\lambda = \lim_{t \to \infty} \ln \left| \frac{\mathcal{D}_i(t)}{\mathcal{D}_i(0)} \right|,$$
(28)

and we understand $t \to \infty$ as long times after the perturbing kick is made to the orbit. When the system is chaotic, nearby trajectories diverge beyond the validity of the linear approximation governing the Lyapunov exponent. To compensate for this, all the state variables of laser B are renormalized back to within ϵ of laser A whenever the round state difference grows to a size of 10ϵ:

$$\mathbf{S}_B[i] \leftarrow \mathbf{S}_A[i] + \frac{\mathbf{S}_B[i] - \mathbf{S}_A[i]}{10},$$
(29)

where $\mathbf{S}[i]$ represents the state variables at time step i. Thus calculating the trajectory difference reduces to finding the number of times normalization was performed and the final value of the trajectory differences. The largest Lyapunov exponent is estimated by examining the slope, in the time-asymptotic linear region, of the logarithm of trajectory differences as a function of time. The initial trajectory perturbation will not necessarily lie upon the eigendirection corresponding to the largest exponent, thus the initial stages of the trajectory divergence will have contributions from all the exponents, though the largest Lyapunov exponent dominates the trajectory divergence exponentially quickly. Since we have no direct way of estimating the other exponents, the actual separation between the largest and the rest of the exponents is difficult to estimate.

A. Kerr coefficient

We examine the dependence of the trajectory divergence on the nondimensional nonlinearity coefficient Φ_{nl}. While the other effects considered are important to the dynamics, we identify the nonlinear polarization rotation to be necessary for chaos.

As we see in Figs. 6 and 7 there is a definite increase in the Lyapunov exponent λ as the nonlinear phase shift Φ_{nl} is increased. We see that even for a value of Φ_{nl} equal to the nominal value found in Eq. (25), we get a positive, although small, exponent. As we increase Φ_{nl} beyond the nominal value we get an increasingly larger exponent. We go from a characteristic trajectory divergence time $\tau_c = (1/\lambda)$ of about $\tau_c = 1$ ms for a nominal Φ_{nl}, to $\tau_c = 0.25$ ms for a Φ_{nl} of 1.75 times that of the nominal value. At the largest value of Φ_{nl} we studied, Φ_{nl} was equal to 2.25 times its nominal value, τ_c was about 0.15 ms. These computations were done with no external injection of light into the ring. We also see that the laser intensity also shows significant divergence. Although the intensity Lyapunov exponent is generally about half of the trajectory exponent, it still follows the same pattern of increasing λ with increasing Φ_{nl} and thus an experimenter monitoring only laser intensity should observe the results of these chaotic intensity fluctuations. Even though the Kerr effect only directly influences the polarization angle, in the whole ring system it leaks out to generate chaos in the intensity as well.

The trend of λ with changing Φ_{nl} (Fig. 7) reveals a generally linear, and certainly monotonic, dependence of λ on Φ_{nl} for both metrics. The error bars were calculated by look-
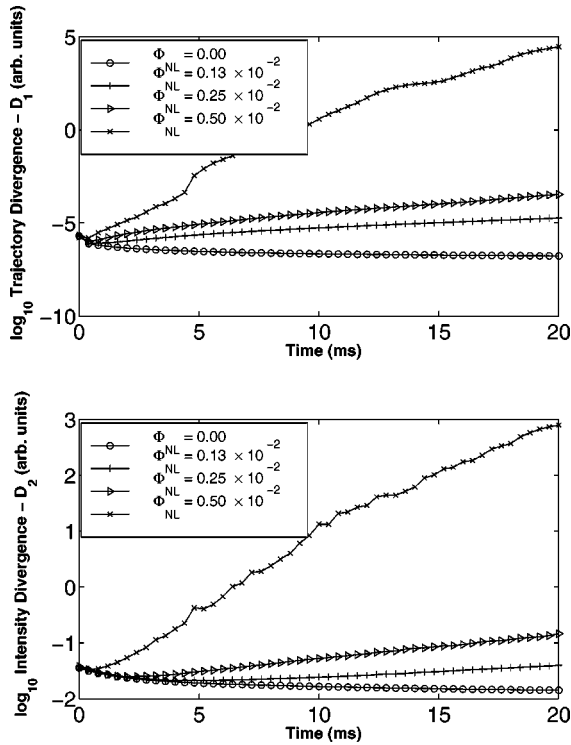
FIG. 6. Trajectory divergences with Φ_{nl} varying from zero to 0.5×10^{-2}. This is a laser with a single loop with no external injection. Here, $\Delta n \approx 2.0 \times 10^{-6}$, and the transmission coefficients are $R_x = 0.9$ and $R_y = 0.85$.

FIG. 7. Trajectory (upper) and intensity (lower) Lyapunov exponents λ varying Φ_{nl}. This is a laser with a single loop and no external injection. Here, $\Delta n \approx 2.0 \times 10^{-6}$, and the transmission coefficients are $R_x = 0.9$ and $R_y = 0.85$.

B. Δn — Linear birefringence

The linear birefringence term results from a net difference in the refractive index experienced by the two electric field polarizations as they travel through the fiber. This contributes only linearly to the dynamics, and thus will not lead to chaotic dynamics on its own. This fact is confirmed numeri-

ing at the standard deviation of the entire group of exponents found if the linear fit is calculated subsequently over the range of starting points between 4 and 16 ms and using an ending point of 20 ms. This measurement gives an estimation of the variance of the exponent calculation depending upon where you look for a best linear slope. Thus we conclude for the apparent relationship between Φ_{nl} and λ that it is valid to consider the Kerr effect as the source of the chaotic behavior in the single-loop EDFRL. Even though the nonlinear polarization rotation conserves optical power in a single pass through an ideal nonlinear medium, the overall system produces chaos in the intensity even when $\Delta R = 0$, i.e., equal transmission coefficients for both polarizations.

The actual value of λ is altered by other effects in the laser, though, as can be seen from Fig. 8. Although there is substantial trajectory and intensity divergence for a Φ_{nl} of 1.5 times the nominal value, we see that a nonzero Δn and a breaking of the transmission coefficient symmetry, ΔR, both serve to increase the exponent value. As shown in the figure, breaking the symmetry in transmission coefficient between polarization states has a small effect if Δn is set to zero. However, if Δn is raised to a physically reasonable value, we see an almost threefold increase in λ in this case. Now when the reflectance symmetry is broken, we get a fourfold increase from the $\Delta n = \Delta R = 0$ case. So while the Kerr nonlinear phase shift is the prime initiator of the chaos, the other linear effects do serve to emphasize the divergences and give higher λ values. Different R_x and R_y turn intensity-dependent polarization rotations into nonlinear intensity fluctuations after a full propagation.
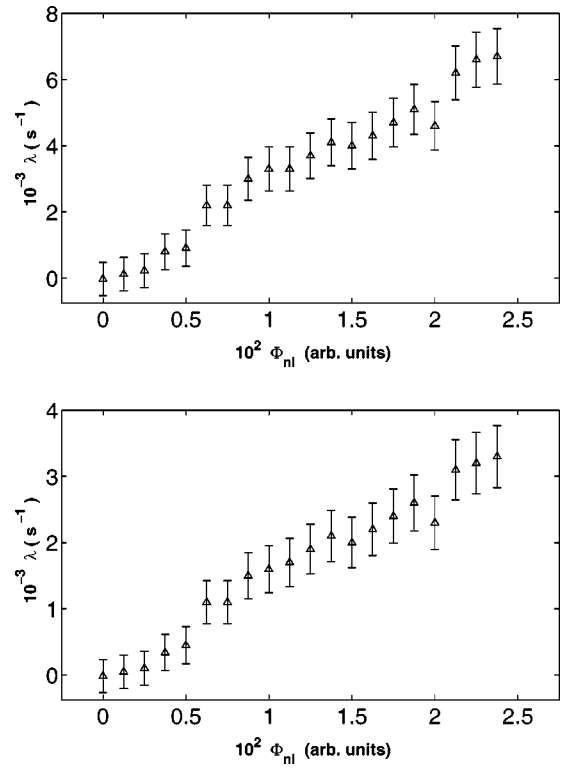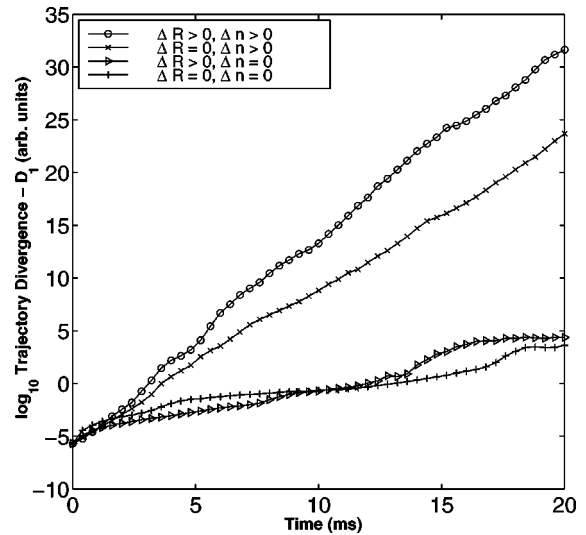

FIG. 8. Dependence on trajectory and intensity divergence for varying values of Δn and ΔR. When $\Delta n > 0$ we use $\Delta n \approx 2.0 \times 10^{-6}$, and when $\Delta R > 0$ we use $R_x = 0.9$ and $R_y = 0.85$. This is a laser with a single loop and no external injection. Here, $\Phi_{nl} \approx 1.5 \times 10^{-2}$.
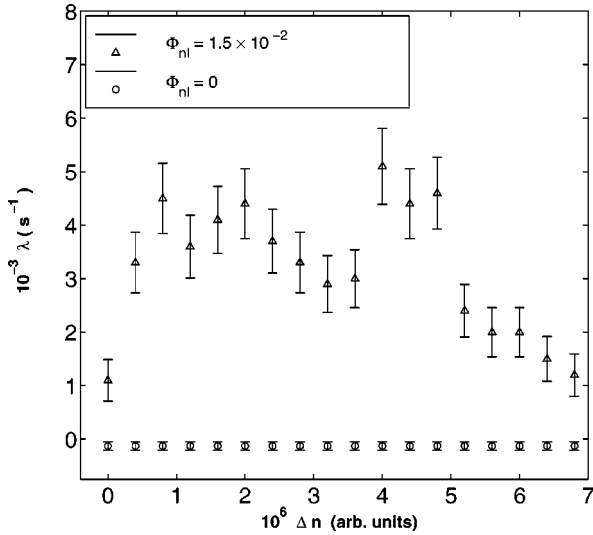
FIG. 9. Lyapunov exponents varying Δn, with and without Kerr nonlinearity. This is a laser with a single loop and no external injection.

cally by the lower curve in Fig. 9 where we see uniform convergence for all values of Δn. Naturally this convergence is characterized by a negative λ, and occurs for all in a wide range of Δn values when the Kerr phase shift Φ_{nl} is set to zero.

However, when the Kerr phase shift is nonzero, variation of the linear birefringence term was found to profoundly influence the value of λ. The upper curve of Fig. 9 shows that varying Δn has a substantial effect on the trajectory and intensity values of λ at fixed Φ_{nl}, though without any clear trend in Δn, unlike Φ_{nl}. Further explorations of the Δn-Φ_{nl} phase space will be necessary if a more complete exploration of the effect on λ of Δn with nonzero Φ_{nl} is desired. Because the common single-mode fibers have random linear birefringence, which is further influenced by the arbitrary mechanical stresses of the fiber in a laboratory, the magnitude of the Lyapunov exponent may be difficult to exactly reproduce experimentally, even if Φ_{nl} can be accurately controlled.

C. External injection

Driving a nonlinear system by a periodic external force often leads to a rich set of bifurcation phenomena in the amplitude, frequency plane of the driving parameters. We certainly expect the same when we drive the ring laser with an external injection of light of certain amplitude and frequency. We examine the case of external injection with Φ_{nl} set to zero in Fig. 10. As in the Δn case, we see uniform trajectory and intensity convergence for a wide range of injection amplitudes. It appears as though we again have the case where there is no trajectory divergence if there is no Kerr effect.

We now examine the effect of outside forcing through injection of light from an external laser into the cavity at fixed Δn and nonzero Φ_{nl}. For these we choose to provide a large λ using $\Phi_{nl}=1.5\times10^{-2}$ and Δn of $\approx2.0\times10^{-6}$. These resulted in $\lambda\approx4100$ s^{-1}. We now choose the detuning between the external laser frequency and the optical frequency of the ring laser $\omega_I-\omega_0\approx16/\tau_R$. In Fig. 10 we see
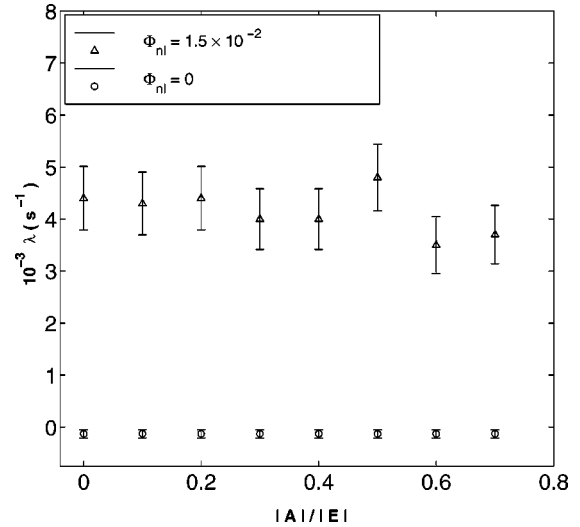

FIG. 10. Lyapunov exponents with varying amplitude of external injection. A single-loop laser with external injection period approximately 1/16 of a round trip, with $\Delta n\approx2.0\times10^{-6}$ and transmission coefficients are $R_x=0.9$ and $R_y=0.85$. X axis is ratio of injected field magnitude to average total field magnitude.

that over a range of injection amplitudes ≈17–77% of the average circulating electric field amplitude in the ring leads to little variation in λ.

On the whole we see similar behavior when we vary the detuning frequency. Taking the same parameters for Φ_{nl} and Δn and an injection amplitude about 55% of the average electric field magnitude, we see in Fig. 11 that the detuning frequency also has little effect on the Lyapunov exponent, for frequencies above ≈5 per round-trip. For smaller frequencies, we see that the chaos is absent, even for values of Φ_{nl} and Δn which gave large λ.

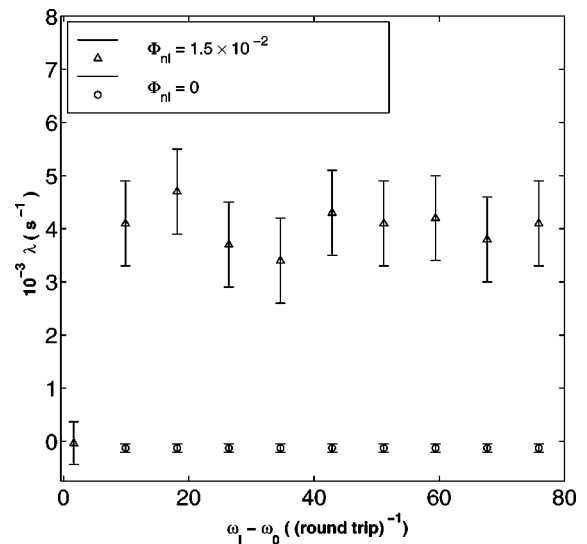Whether this is physically important depends on the range of parameters which are experimentally realizable. In the ex-

FIG. 11. Lyapunov exponents with varying frequency of external injection. This is a laser with a single loop with injection amplitude $\approx55\%$ of field amplitude. Here, $\Phi_{nl}=1.5\times10^{-2}$, $\Delta n\approx2.0\times10^{-6}$ and the transmission coefficients are $R_x=0.9$ and $R_y=0.85$.

perimental situation of Roy and VanWiggeren [6,8], such a slow detuning frequency due to external injection is not one which could be realized consistently, since the EDFRL lases over a frequently changing range of wavelengths. So for injection frequencies which are in a physically meaningful range, λ is essentially unaffected by changes in the detuning.

D. Summary of variations in chaotic behavior

We conclude that in the case of a single-loop EDFRL, the origin of chaotic oscillations is clearly the nonlinear Kerr effect which mixes polarizations while preserving intensities. The positive Lyapunov exponent λ associated with nonzero Φ_{nl} varies more or less linearly in Φ_{nl} over the range we explored, and it varies substantially with the magnitude of linear birefringence. λ appears to be relatively insensitive to the amplitude and detuning frequency associated with external injection into the laser cavity, though there are frequency values where the ring laser locks into periodic behavior and λ→0. By no means does our small investigation cover the range of phenomena which may appear in the parameter space formed by Δn, Φ_{nl}, injection amplitude, and $\omega_I - \omega_0$.

VI. TWO-RING EDFRL

VanWiggeren and Roy [8] also investigated the oscillations of a ring laser when a second loop of passive fiber was added to the ring. This adds a second time delay to the ring laser system and it affects the polarization of the light. When light arrives at the entrance to the second loop a fraction α of its electric field enters the new ring and 1 − α continues on in the new ring. The light in the second ring is propagated as described in detail above and encounters a Jones matrix $\mathbf{J}_{loop}$ on circulating about the loop. As the light from the second loop reenters the main ring, it is added to light in the main ring which has not undergone a propagation over the round-trip time of the second loop τ_D. This means we should replace the propagation equation we had before (absent external injection which is not affected by the new loop) by

$$\mathcal{E}(t+\tau_R) = \mathbf{R} e^{i\omega_0 n_0 l_F/c} \mathbf{J}'_{PC} \mathbf{U}_{whole\ fiber}[(1-\alpha)\mathsf{P}\{\mathcal{E}(t)\}$$
$$+ \alpha \mathbf{J}_{loop}\mathsf{P}\{\mathcal{E}(t+\tau_D)\}]. \qquad (30)$$

This expression for the effect of the second loop of length $\tau_D c$ cannot be represented solely by a redefinition of the Jones matrix of the first loop. One can see this by noting that even at $\tau_D = 0$, the effect of the second loop is not given by a unitary matrix in general.

A. Examples of the two-ring EDFRL operation

The introduction of a second loop significantly changes the outward character of the laser oscillations. The time series looks quite periodic, but on much smaller time scales than in the single-loop configuration. This is shown in Fig. 12. With a single loop, the intensity was almost periodic with a period of τ_R, but with the second loop activated, there are about 45 periods within one round-trip when the τ_D is slightly less than half of τ_R. The frequency spectrum is also changed, and with the second loop there is much more power in a few frequencies as one may see in Fig. 13. In the case
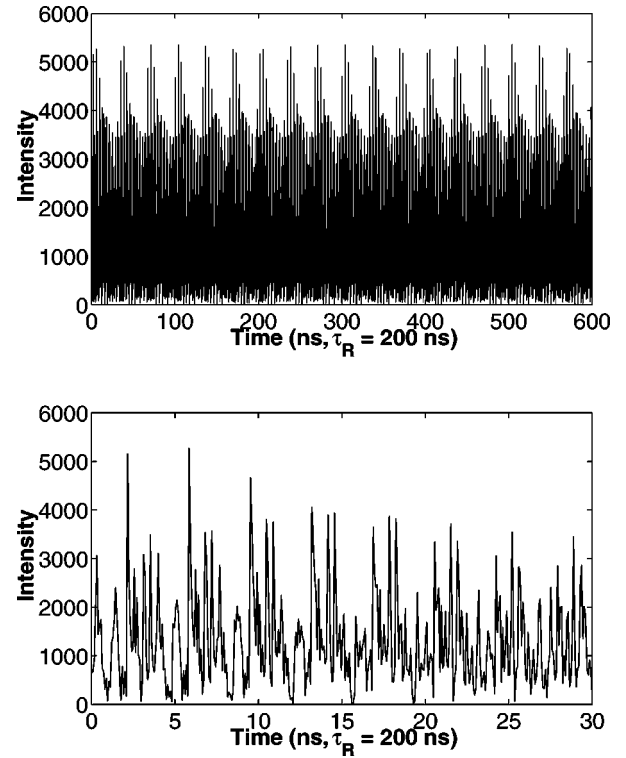

FIG. 12. A time series of the output of the laser simulation with a second loop. In the lower graph one can see a near periodicity on very small time scales. This is a laser with no external injection. Here, $\tau_D/\tau_R = 0.4468$, the coupling to the second loop is 0.1, $\Delta n \approx 2.0 \times 10^{-6}$, the pumping is at $11\times$ threshold, and the reflectances are $R_x = 0.9$ and $R_y = 0.85$.

where the second Jones matrix is the identity, the cause of this effect can be seen by thinking of the second loop as the insertion of a FIR filter into the ring with the first coefficient $1 - \alpha$, α after a delay of τ_D, and all other coefficients zero. The transfer function of such a filter is

$$H(\omega) = (1-\alpha) + \alpha e^{-i\omega\tau_D}. \qquad (31)$$

Thus the second loop attenuates all frequencies not commensurate with the delay loop. Because most of the power is in the harmonics of one round-trip, those harmonics that are close to commensurate with the delay are given much more power. To remove this apparent periodicity, we made a stroboscopic section, sampling the intensity once per $10\tau_R$ instead of 2500 times per τ_R. The result removes all of the harmonics of $1/\tau_R$ and is aperiodic. The result of this is seen in Fig. 14.

Ignoring nonlinearity for a moment, the net effect of having a second loop is for the system to try to find a state which is approximately commensurate with both the round-trip times of both paths. Most commonly, the system evolves a periodic signal whose period is significantly shorter than either round-trip, so that an integral number of these short periods can fall through either loop and recombine constructively. This explains the dominant visual difference between the one- and two-ring simulation results.

B. Chaos in the two-ring EDFRL

Using the methods described above, we evaluated λ for the two-ring system. We found that the introduction of the
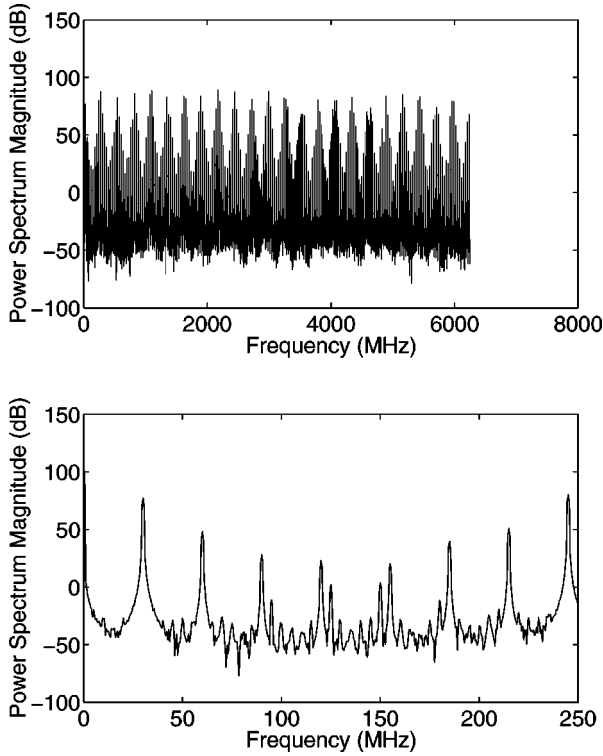
FIG. 13. Top: power spectrum of the output of the laser simulation with a second loop. Here, $\tau_D/\tau_R=0.4468$, the coupling to the second loop is 0.1, $\Delta n \approx 2.0 \times 10^{-6}$, the pumping is at $11\times$ threshold, and the reflectances are $R_x=0.9$ and $R_y=0.85$.

second loop has a dramatic effect on the largest Lyapunov exponent.

Figure 15 shows the Euclidean distance $\mathcal{D}_1$ between two close trajectories for several different values of the coupling between the two loops including $\alpha=0$, that is, with the second loop decoupled from the first. Figure 16 is similar to Fig. 15, but we have increased the pump level into the first ring by a factor of about 2, and Φ_{nl} was increased to 1.5 times its nominal value. The increased pumping also serves to in-
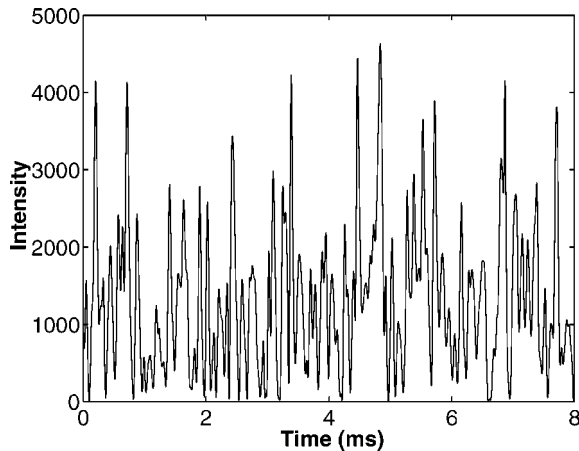
FIG. 14. A stroboscopic section of the two-loop laser with the sampling rate once per $10\tau_R$. As before the lack of periodicity on a long time scale can be seen. There is no external injection. Here, $\tau_D/\tau_R=0.4468$, the coupling to the second loop is 0.1, $\Delta n \approx 2.0 \times 10^{-6}$, the pumping is at $11\times$ threshold, and the reflectances are $R_x=0.9$ and $R_y=0.85$.
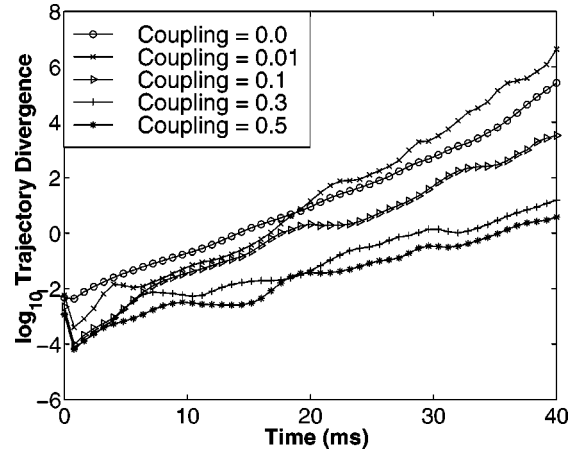

FIG. 15. Trajectory divergences with varying coupling to the second loop. This is a laser with no external injection. Here, $\tau_D/\tau_R=0.4468$, $\Delta n \approx 2.0 \times 10^{-6}$, the pumping is at $11\times$ threshold, $\Phi_{nl}=5.0 \times 10^{-3}$, and the reflectances are $R_x=0.9$ and $R_y=0.85$.

crease the magnitude of the Kerr effect, as it increases the amount of power in the laser. In both cases, as the amount of light put in the second loop increases, the highest Lyapunov exponent decreases. However, in both cases the largest λ came from a two-loop, not a one-loop, ring laser.

Despite the large effect the difference in indices of refraction had in the single-loop case, it seemed to have little or no effect in the two-loop case. Figure 17 shows the trajectory divergence for a range of Δn and there is not much change in the slope. The slopes do vary somewhat, but the uncertainty in the calculation of the slopes is also large. Changing the length of the second loop changes the highest Lyapunov exponent. Figure 18 shows the trajectory divergence for several delay times τ_D. The slope varies with the delay time irregularly, much as it did for varying Δn in the single-loop case.

The other metrics for measuring trajectory divergence did not behave very differently from the Euclidean metric. The slopes using metric $\mathcal{D}_2$ were half those of $\mathcal{D}_1$. The physical conclusion is that the chaos is uniformly mixed in phase and
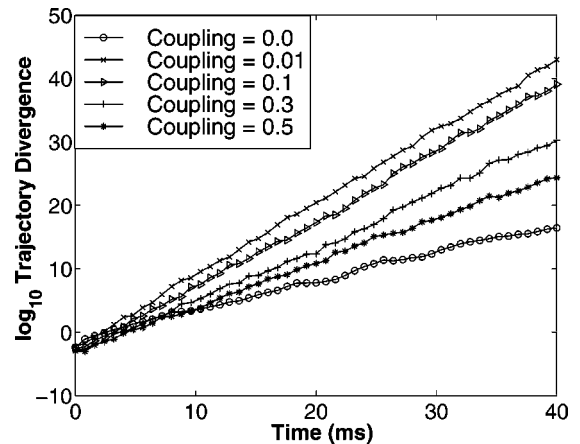

FIG. 16. Trajectory divergences with varying coupling to the second loop and greater pumping. This is a laser with no external injection. Here, $\tau_D/\tau_R=0.4468$, $\Delta n \approx 2.0 \times 10^{-6}$, the pumping is at $20\times$ threshold, $\Phi_{nl}=1.5 \times 10^{-2}$, and the reflectances are $R_x=0.9$ and $R_y=0.85$.
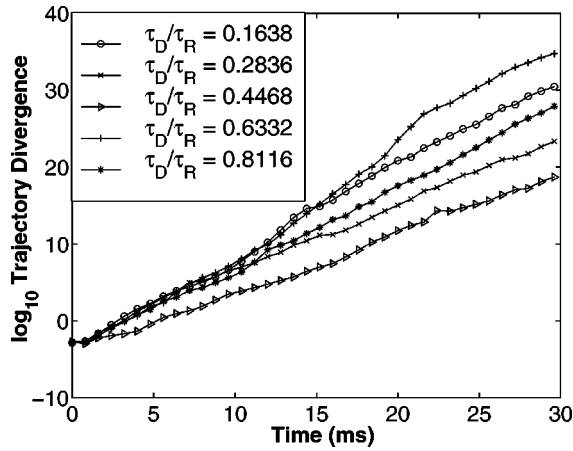
FIG. 17. Trajectory divergences with varying Δn. As in the single-loop case, the highest exponent does have a simple dependence on Δn. This is a laser with a double loop and no external injection. Here, $\tau_D/\tau_R = 0.4468$, the coupling to the second loop is 0.1, the pumping is at $11\times$ threshold, $\Phi_{nl} = 5.0\times10^{-3}$, and the reflectances are $R_x = 0.9$ and $R_y = 0.85$.

FIG. 18. Trajectory divergences with varying delay in the second loop. There is no simple dependence of the highest Lyapunov exponent on τ_D. This is a laser with no external injection. Here, the coupling to the second loop is 0.1, $\Delta n \approx 2.0\times10^{-6}$, the pumping is at $20\times$ threshold, $\Phi_{nl} = 1.5\times10^{-2}$, and the reflectances are $R_x = 0.9$ and $R_y = 0.85$.

intensity, the particular difference being only in the definitions of the metrics.

VII. CONCLUSIONS AND DISCUSSION

This paper has been the first in a pair [10] investigating synchronization and communication between realistic model erbium-doped fiber ring lasers. We plan to discuss synchronization and communication in the future while this paper has been devoted to the dynamics of an individual EDFRL.

In order to account for the dynamics of a very slowly changing population inversion compared to the round-trip time of light through the fiber ring, we focused on three dynamical effects which might appear to be of little interest for a single round-trip: group velocity dispersion, linear birefringence, and terms in the polarization of the medium cubic in the electric field; the Kerr effect.

Each of these had a major effect on the electric field and intensity of the light circulating in the fiber ring when we looked at many hundreds of thousands of round-trip times of that light. This scale of round-trip times is dictated by the ratio of lifetime of the lasing state, about 10 ms, and the optical cavity round-trip time, about 200 ns. The main role of GVD during this large number of round-trips was to remove high-frequency components from the initial state of the electric field. The linear birefringence had a substantial effect in separating the dynamics of the two polarizations, and the key role played by the Kerr effect was to create conditions where chaotic oscillation of the electric field was possible. We developed numerical techniques to permit rapid simulation over long integration times, compared to explicit integration of the underlying wave equations.

Nonlinearity in the dynamics of the EDFRL appears only in the Kerr terms associated with the polarization of the medium and in the equation for the population inversion. The latter is effectively constant during many hundreds of thousands of round-trips, so the principal source of nonlinear dynamics in this laser comes from the Kerr terms. We have shown quite explicitly in our simulation that when this term
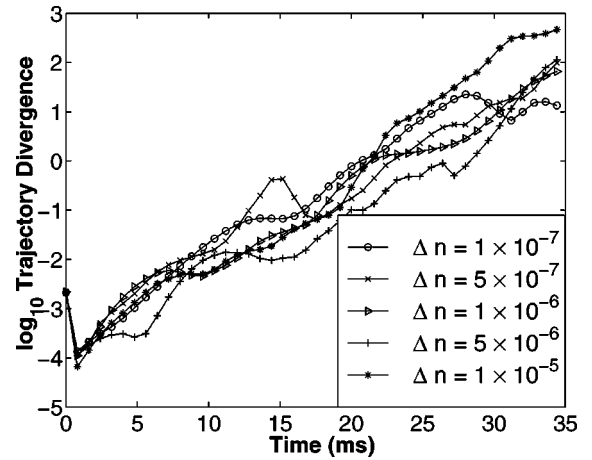
is set to zero, the effective Lyapunov exponent λ associated with trajectory divergences is zero. When we increase Φ_{nl}, which is proportional to χ_3, the Kerr term, λ becomes positive even for values less than that known for pure fused silica. This is a clear indication that chaos in the operation of this kind of laser arises from this optical nonlinearity.

We investigated the dependence of λ on linear birefringence and on the amplitude and frequency of externally injected light and found that usually positive Φ_{nl} lead to chaotic behavior. The exceptions involve some circumstances with externally injected monochromatic light which cause locking in the ring laser operation. In these cases $\lambda = 0$.

The stage is set now for two directions of investigation.

(1) Couple two EDFRLs using the schemes discussed in [7]. This is the subject of our companion paper [10].

(2) Change the doping material to Nd or Pr which alters three important parameters in this problem: (1) the relaxation time of these rare earths is less by about a factor of 10:100 μs for Pr and 400 μs for Nd. (2) The wavelength of interesting laser action is about 1.3 μm which is within another important communications window, and (3) the GVD coefficient β_2 is nearly zero at this wavelength.

Our simulations of the EDFRL also raise the issue of experimental verification of the dependence of the largest Lyapunov exponent on the nonlinear phase shift Φ_{nl} or equivalently on the nonlinear optical effects of χ_3. We plan to report [20] on our investigations of this in the near future. The collection of experimental data in this regard requires some care as the very large ratio of fluorescence lifetime to cavity round-trip time means the wave forms whose chaotic oscillations we are investigating change on a quite slow time scale compared to all other phenomena in this system.

[1] R.J. Mears, L. Reekie, I.M. Jauncey, and D.N. Payne, Electron. Lett. **23**, 1026 (1987); H. Takara, S. Kawanishi, M. Saruwatari, and K. Noguchi, *ibid.* **28**, 2095 (1992); Th. Pfeiffer and G. Veith, *ibid.* **29**, 1849 (1993).

[2] *Selected Papers on Rare-Earth-Doped Fiber Laser Sources and Amplifiers*, edited by M.J.F. Digonnet, SPIE Milestone Series Volume MS 37 (SPIE, Bellingham, WA, 1992).

[3] Anders Bjarklev, *Optical Fiber Amplifiers: Design and System Applications* (Artech House, Boston, 1993).

[4] Q.L. Williams and R. Roy, Opt. Lett. **21**, 1478 (1996); Q.L. Williams, J. Garcia-Ojalvo, and R. Roy, Phys. Rev. A **55**, 2376 (1997); J. Garcia-Ojalvo and R. Roy, Phys. Lett. A **229**, 362 (1997).

[5] W.H. Loh and C.L. Tang, IEEE J. Quantum Electron. **27**, 389 (1991); W.H. Loh, Y. Ozeki, and C.L. Tang, Appl. Phys. Lett. **56**, 2613 (1990); W.H. Loh and C.L. Tang, Opt. Commun. **85**, 283 (1991).

[6] R. Roy and G. VanWiggeren, Science **279**, 1198 (1998).

[7] H.D.I. Abarbanel and M.B. Kennel, Phys. Rev. Lett. **80**, 3153 (1998).

[8] G. VanWiggeren and R. Roy, Phys. Rev. Lett. **81**, 3547 (1998).

[9] R. Roy and G. VanWiggeren (private communication).

[10] C.T. Lewis, H.D.I. Abarbanel, M.B. Kennel, M. Buhl, and L. Illing (unpublished).

[11] K. Ikeda, Opt. Commun. **30**, 257 (1979); K. Ikeda, H. Daido, and O. Akimoto, Phys. Rev. Lett. **45**, 709 (1980).

[12] G.H.M. van Tartwijk and G.P. Agrawal, Prog. Quantum Electron. **22**, 43 (1998).

[13] For some examples and references to others, see the special issue of IEEE Trans. Circuits Syst. I: Fundam. Theory Appl. **44**, 853 (1997), edited by M.P. Kennedy and M. Ogorzalek.

[14] N.F. Rulkov and A.M. Volkovskii, Pis'ma Zh. Tekh. Fiz. **19**, 42 (1993) [Tech. Phys. Lett. **19**, 17 (1993)].

[15] G.P. Agrawal, *Nonlinear Fiber Optics*, 2nd ed. (Academic Press, San Diego, 1995).

[16] Joseph T. Verdeyen, *Laser Electronics*, 3rd ed. (Prentice-Hall, Englewood Cliffs, NJ, 1995).

[17] G.P. Agrawal, Phys. Rev. A **44**, 7493 (1991).

[18] C.D. Poole and R.E. Wagner, Electron. Lett. **22**, 1029 (1986).

[19] H. Winful, Appl. Phys. Lett. **47**, 213 (1985).

[20] H.D.I. Abarbanel, M. Buhl, M.B. Kennel, C.T. Lewis, R. Roy, and G. VanWiggeren (unpublished).

[21] H.D.I. Abarbanel, *Analysis of Observed Chaotic Data* (Springer, Berlin, 1996).